



2020

Stability and Evolution of Planar and Concave Slopes under Unsaturated and Rainfall Conditions

Arash Hassanikhah
ahassani@utk.edu

Eric C. Drumm
edrumm@utk.edu

Follow this and additional works at: https://trace.tennessee.edu/utk_biospubs



Part of the [Bioresource and Agricultural Engineering Commons](#), and the [Geotechnical Engineering Commons](#)

Recommended Citation

Hassanikhah, Arash and Drumm, Eric C., "Stability and Evolution of Planar and Concave Slopes under Unsaturated and Rainfall Conditions" (2020). *Biosystems Engineering and Soil Science Publications and Other Works*.

https://trace.tennessee.edu/utk_biospubs/13

This Article is brought to you for free and open access by the Biosystems Engineering and Soil Science at Trace: Tennessee Research and Creative Exchange. It has been accepted for inclusion in Biosystems Engineering and Soil Science Publications and Other Works by an authorized administrator of Trace: Tennessee Research and Creative Exchange. For more information, please contact trace@utk.edu.



University of Tennessee, Knoxville
**Trace: Tennessee Research and Creative
Exchange**

Biosystems Engineering and Soil Science
Publications and Other Works

Biosystems Engineering and Soil Science


2020

Stability and Evolution of Planar and Concave Slopes under Unsaturated and Rainfall Conditions

Arash Hassanikhah

Eric C. Drumm

Follow this and additional works at: https://trace.tennessee.edu/utk_biospubs

 Part of the [Bioresource and Agricultural Engineering Commons](#), and the [Geotechnical Engineering Commons](#)

Stability and Evolution of Planar and Concave Slopes under Unsaturated and Rainfall Conditions

Arash Hassanikhah, M. ASCE¹ and Eric C. Drumm, M. ASCE²

¹Postdoctoral Research Associate, Dept. of Biosystems Engineering and Soil Science, University of Tennessee, Knoxville, TN 37996

²Professor, Dept. of Biosystems Engineering and Soil Science, University of Tennessee, Knoxville, TN 37996 (corresponding author). E-mail: edrumm@utk.edu

Abstract:

Natural slopes are often observed to have a concave, convex, or a combination concave/convex profile, yet constructed slopes are traditionally designed with planar cross-sectional geometry. In this paper, the stability of two planar slopes was compared with that of companion concave slopes, designed to have similar factors of safety (FOS) under gravity loading. The stability of these slopes was then investigated in response to a suction event followed by a precipitation event, and it was shown that both the planar and the concave slopes experienced similar changes in stability. Additional analyses were conducted with a simulated erosion mechanism to investigate how the planar and concave shapes would evolve under a sequence of three similar suction/precipitation/erosion cycles. The results suggest that for these slopes, the second and third simulated weather cycles reduced the stability of the slopes, yet had a lesser effect on the concave slopes than the planar slopes. This is in spite of the fact that the planar slopes became more "concave-like" due to the simulated erosion, and suggests slopes designed to be concave may perform better than the planar slopes.

Keywords: Planar slope, soil suction, unsaturated slope, soil viscosity, limit equilibrium, shear strength reduction factor.

30 **Introduction:**

31 Most constructed slopes, both cut and fill slopes, are designed with a planar cross-section geometry
32 (uniform gradient), which while being more straightforward for analysis and construction, does not
33 produce natural appearing earth structures. The natural, sustainable shape of a slope could be concave,
34 convex, or a combination of concave and convex (Schor and Gray, 2007). A conceptual model of slope
35 evolution from a planar shape to a concave shape indicates that both mass stability analysis and surficial
36 erosion processes enable a stable shape to be created for given soil properties (Gray, 2013). The driving
37 forces, material properties, and slope geometry are the determinant parameters in the mass stability
38 analysis, and govern the factor of safety (FOS) of the slope. In a planar slope, the driving force increases
39 linearly from top to bottom of the slope, and the tractive force due to erosion also increases with the
40 distance downslope. However, as described by Schor and Gray (2007), in a concave slope, the driving force
41 decreases from top to bottom as the angle of the slope gradually decreases, and the tractive force exerted
42 by the runoff also decreases as the slope decreases. A concave slope having a constant rate of erosion
43 down the slope reaching steady-state equilibrium while maintaining mechanical stability has been
44 suggested as an optimal slope shape (Jeldes et al. 2018). A uniform rate of erosion may lead to parallel
45 retreat of some concave slopes. Hancock et al. (2003) argued that a compound shape can be described
46 using an area-slope relationship, which is the relationship between the drainage area and slope of a point
47 on the slope.

48 Stability analyses of concave slopes have been conducted based on slip-line theory, limit equilibrium
49 method, and limit analysis approach. Utili and Nova (2007) utilized an upper bound method of limit
50 analysis to reach an optimal log spiral profile of a slope yielding a maximum safety factor for given average
51 slope angle or given soil properties. Jeldes et al. (2013) simplified the Sokolovskii (1960, 1965) slip-line
52 theory solution using an analytical approximation to reach an optimum concave slope shape based on the
53 effective shear strength parameters, total soil unit weight and the slope height. The theoretical

54 mathematical solution for this method produces a sharp vertical edge at the top of the slope or "cusp"
55 based on the tension crack depth, and it was suggested that the cusp may be an unstable and temporary
56 component of the slope in many cases. The erosion of concave slopes was shown to be lower than that in
57 equivalent planar slopes, and a design procedure was suggested (Jeldes et. al 2015). Vahedifard et al.
58 (2016) used a geometric technique incorporating a limit equilibrium formulation to develop stability
59 numbers for a wide range of circular concave slopes including the effects of the upper inclined slope
60 surface. The inclined surfaces with different angles were considered as an upper component of the slope
61 and they concluded that the increase of the upper slope angle or the cusp formation resulted in an
62 unstable situation for slopes. Vo and Russell (2017) investigated the role of soil suction in unsaturated
63 non-planar slopes in and developed a series of stability charts in dimensionless form.

64 In this paper, two "virtual" or contrived slopes taken from the literature, along with equivalent companion
65 concave slopes, are evaluated by the Finite Element method to investigate the effect of shape and the
66 evolution of slope shape during a series of weather cycles. Here, a companion slope is defined as one with
67 the same height and material properties but with a concave shape defined according to Jeldes et al.
68 (2013). The stability of the slopes is evaluated under gravity alone, then the application of soil suction or
69 a drying event, followed by a constant intensity rainfall event. Specifically, the following are addressed:

- 70 • The stability and change in the FOS of both planar and concave slopes due to reduction of
71 unsaturated soil strength caused by a precipitation event
- 72 • The evolution of both planar and concave slope geometry as a series of precipitation events
73 reduces the surficial soil suction and strength, allowing the material to be eroded and lost from
74 the slope.

75 The intent of the investigation was not to evaluate the effect of specific hydraulic characteristics (Cai
76 and Ugai 2004) or model the erosion process (Jeldes et al. 2018). Instead, the intent was to investigate
77 how both planar and concave companion slopes might generally respond to an arbitrary drying and

78 rainfall event, and how the shape of the slopes may evolve over a series of these cycles. The goal was to
79 see if a concave shape was sustainable, and if the sharp cusp at the top of slope was likely to be a
80 temporary feature that exists due to the mathematics of the soil tensile strength.

81 In addition to the above, the convergence criteria of the coupled hydro-mechanical visco-plastic model
82 used to represent the soil in the unsaturated slopes is described, along with other details of the
83 numerical approach.

84 **Numerical investigation of the stability of planar and equivalent concave slopes**

85 In this paper, the mechanical stability of two planar slopes with different geometries and mechanical
86 material properties was investigated under gravity load to obtain the initial design FOS as identified by
87 the Shear Strength Reduction Technique (SSRT) (e.g. Zienkiewicz et al. 1975; Griffiths and Lane, 1999).
88 This method has been used in both FEM and LE methods and the FOS obtained in the SSRT corresponds
89 to the Strength Reduction Factor (SRF) at which the slope would fail, or the ratio of the actual shear
90 strength of the soil to the lowest shear strength at which failure occurs. The analysis is conducted using
91 factored shear strength parameters c'_f and ϕ'_f (and ϕ^b_f)

$$92 \quad c'_f = \frac{c'}{SRF}, \phi'_f = \arctan\left(\frac{\phi'}{SRF}\right) \text{ and } \phi^b_f = \arctan\left(\frac{\phi^b}{SRF}\right) \quad (1)$$

93 where c' is the effective cohesive strength, ϕ' is the effective internal friction angle, and ϕ^b is the internal
94 friction angle with respect to suction. Failure is reached by gradually and systematically increasing the
95 SRF, thus obtaining the FOS. The FOS's from the planar slopes are then used to determine the shape of
96 companion concave slopes based on the analytical equations proposed by Jeldes et al. (2013). The
97 coordinates of the companion concave slopes are obtained based on the density, γ , slope height, H_s , and
98 the factored strength parameters c'_f and ϕ'_f of the companion slope. This produces a concave slope with

99 essentially the same FOS as the original planar slope. The coordinates of the concave slope are described
 100 (Jeldes et al. 2013) as:

$$101 \quad x = \begin{cases} 0, & -h_{cr} \leq y \leq 0 \\ A[\sigma_y(B-1)(\operatorname{cosec} \phi - 1) + p_t B (\operatorname{cosec} \phi + 1)], & y > 0 \end{cases} \quad (2)$$

102 where

$$103 \quad A = \frac{\cos \phi}{2\gamma(1-\sin \phi)} \quad (3)$$

$$104 \quad B = \ln \left[\frac{\sigma_y}{p_t} \left(\frac{1-\sin \phi}{1+\sin \phi} \right) + 1 \right] = \ln \left[\frac{\sigma_y}{p_t} K_a + 1 \right] \quad (4)$$

$$105 \quad h_{cr} = \frac{2c \cos \phi}{\gamma(1-\sin \phi)} \quad (5)$$

106 with $\sigma_y = \gamma y$ or the geo-static vertical stress, and $p_t = c' \cot \phi$. Note that p_t is the tensile strength of the soil,
 107 $K_a = (1 - \sin \phi)/(1 + \sin \phi)$ is the Rankine active coefficient of earth pressure, and h_{cr} is the height of
 108 the tension zone. The equation describes a slope contour in the quadrant with x-axis positive to the right
 109 and y-axis positive downward, with h_{cr} lying above the x-axis from the coordinates (0,0) to (0,- h_{cr}). Notice
 110 that this h_{cr} tension zone does not contribute to resistance, but only to destabilization.

111 The two slopes are designated as Slope 1 (of moderate inclination) and Slope 2 (of steep inclination) and
 112 were adapted from the literature (Le et al. 2015, and 2016; Jeldes et al. 2015, respectively). Slope 1 (Fig.
 113 1a) was selected as an example of a slope that was only moderately stable in the absence of the soil
 114 suction (Le et al. 2015). Slope 2 (Fig. 1b) was selected as the stability and erosivity were compared with
 115 an equivalent concave slope (Jeldes 2015).

116 Slope 1 has a height of 10 m and an inclination angle of 26.5° while Slope 2 has a height of 15 m and an
 117 inclination angle of 41° , and both slopes have a water table surface assumed to be at a depth of 15 m
 118 from the top of the slope. The pore water pressure is assumed to be distributed hydrostatically (linearly)
 119 from the water table surface toward the lowest and the uppermost levels as positive or negative values,
 120 respectively. The negative value, referred to as suction, exists for a height of 15 m in both slopes, which

121 is a typical depth of the wetting and active zone in arid and semiarid regions (Nelson et al. 2001). This
122 corresponds to an assumed suction value of 150 kPa at the ground surface in both slopes. The stability of
123 the two slopes was investigated under the gravitational loading, followed by a 5-day period of drying or
124 application of the suction, which was then followed by a significant precipitation event with a rate of 43.2
125 mm/day (5^{-4} kg/m²/s) with duration of 5 days applied through the ground surface. This rainfall event is
126 consistent with that investigated by Le et al. (2015).

127 The analyses were performed with the finite element code Code Bright (DIT-UPC, 2015), which couples
128 the hydraulic and mechanical properties of the soil. The mechanical material properties were taken from
129 the original references for each of the slopes, to allow for direct comparison with the previously published
130 FOS results. In order to better compare the response during the drying and precipitation events, the two
131 slopes were assumed to have identical hydraulic properties, with the majority of the hydraulic properties
132 taken from the Slope 1 references (Le et al. 2015, 2016). The focus of the analysis was not on the effect
133 of the hydraulic properties on slope stability, as was investigated by Cai and Ugai (2004). Instead, the focus
134 of the paper was on the evolution of the slope shape and the differences in response between the planar
135 and concave slopes, which is better examined if the hydraulic properties were identical. Since there may
136 be some inconsistency between the mechanical parameters and the hydraulic parameters of the two
137 slopes, they may best be considered "virtual" or contrived slopes chosen to compare planar and concave
138 slopes and the evolution in shape of both.

139 Code Bright (DIT-UPC, 2015), employs the net mean stress and suction as main stress variables as:

140 Net stress:
$$\bar{\sigma}_{ij} = \sigma_{ij} - \max(p_g, p_l)\delta_{ij} \quad (6)$$

141 Suction:
$$s = \max((p_g - p_l), 0) \quad (7)$$

142 where: σ_{ij} is the total stress, p_g is the gas or air pressure, which is assumed to be zero, p_l is the water
 143 pressure, and is δ_{ij} the Kronecker delta. By assuming air pressure equal to zero, the net normal stress is
 144 defined as the total stress above the water table and the effective stress below water table.

145 The soil water characteristic curve (SWCC) or the relationships between negative pore water
 146 pressure/suction, s and degree of Saturation, S and the relationship between S and unsaturated hydraulic
 147 conductivity, k_u were chosen to be compatible with van Genuchten's equation (1980). The effective
 148 saturation, S_e , is defined such that it varies between 0 and 1 (Fig. 2a) as

$$149 \quad S_e = \frac{S - S_r}{S_s - S_r} = \left[1 + \left(\frac{s}{s_e} \right)^{1/(1-m)} \right]^{-m} \quad (8)$$

150 where S = degree of saturation; S_r = residual saturation; S_s = maximum saturation; s = suction, s_e = air-
 151 entry suction parameter = $s_e = s_{e0} \exp[\eta(n_0 - n)]$

152 s_{e0} = reference air-entry pressure; η = parameter for the influence of porosity, n , on the SWCC; m = shape
 153 function; and n_0 = reference porosity.

154 The unsaturated hydraulic conductivity, k_u (Fig. 2b) is a function of the effective saturation, S_e , and
 155 porosity, n , and is expressed as

$$156 \quad k_u = k_s k_r \quad (9)$$

157 where k_s = saturated permeability (m/s) and k_r = relative permeability defined as follow:

$$158 \quad k_s = k_{s0} \left[\frac{n^3}{(1-n)^2} \right] \left[\frac{(1-n_0)^2}{(n_0)^3} \right] \quad (10)$$

$$159 \quad k_r = \sqrt{S_e} \left[1 - \left(1 - S_e^{1/m} \right)^m \right]^2 \quad (11)$$

160 where K_{s0} = saturated permeability.

161 Thus, the FEM code varies the permeability as the soil porosity (or volumetric strain) and the saturation
 162 change as defined above. During a rainfall event, the initial negative pore water pressure on the upper

163 surface is reduced due to boundary flow, and the pressure is redistributed below the ground surface based
 164 on the hydraulic conductivity. A negative leakage coefficient γ_l was used as a boundary parameter along
 165 the ground surface to maintain the pore water pressure less than or equal to zero avoiding positive pore
 166 water pressure. Thus the flux, q_l is described both on the boundary and within the slope using the
 167 following flux equations (i.e. Darcy's law):

$$168 \quad q_l = q_{l0} + \gamma_l(p_l + p_{l0}) \quad (12)$$

$$169 \quad q_l = -\frac{Kk_r}{\mu_l}(\nabla p_l + \rho_l g) \quad (13)$$

170 where q_l = water flux (kg/m²/s), q_{l0} = reference water flux (e.g. rainfall), K = intrinsic permeability (m²),
 171 k_r =relative permeability, γ_l = leakage coefficient, μ_l =water viscosity (MPa.s.), ρ_l =water density (kg/m³),
 172 p_l =water pressure (kPa), p_{l0} =reference water pressure (kPa), and g =acceleration due to gravity (m/s²).

173 A visco-plastic model with a Mohr-Coulomb failure criterion, as implemented in the Finite Element code
 174 Code_Bright (DIT-UPC, 2015) was used to model the time-dependent progressive failure. The incremental
 175 stress state in the soil is represented by

$$176 \quad d\sigma_{ij} = D_{ijkl}^e \left(d\varepsilon_{kl} - \delta_{kl} \frac{ds}{K_s} - d\varepsilon_{kl}^p \right) \quad (14)$$

177 where $d\sigma_{ij}$ = incremental stress matrix

178 D_{ijkl}^e = elastic stiffness matrix (isotropic)

179 s = soil suction

180 $d\varepsilon_{kl}$ = the incremental strain

181 K_s = bulk modulus against suction changes

182 $d\varepsilon_{kl}^p$ = incremental plastic strain

183 Yield is defined by the extended Mohr-Coulomb criterion as:

184

$$185 \quad F^P = \left(\cos \theta + \frac{1}{\sqrt{3}} \sin \theta \sin \phi' \right) J \sin \phi' (p + p_t) \geq 0 \quad (15)$$

186 where θ is the Lode angle, J is the square root of the second invariant of deviatoric stress tensor, ϕ' is
 187 the soil friction angle, p is soil net mean stress, and p_t is the soil tensile strength = $c' \cot \phi'$ with c' = the
 188 soil cohesive strength. The shear strength reduction technique (SSRT) was used by incrementing the
 189 reduction factor by 0.01 from 1.0 to the value resulting in failure.

190 The visco-plastic rate dependency is introduced by a plastic multiplier λ^P expressed as a function of the
 191 distance between the current stress point in the soil matrix and the inviscid plastic locus:

$$192 \quad d\lambda^P = (dt/\eta^M) \langle F^P \rangle \quad (16)$$

193 where dt is the time increment, η^M is the soil viscosity, and F^P is the Mohr-Coulomb yield function. The
 194 inviscid plastic locus (\bar{F}^P) is defined as follows:

$$195 \quad \bar{F}^P = F^P - (\eta/dt) d\lambda^P \leq 0 \quad (17)$$

196 where F^P = Mohr Coulomb yield criterion (eq 15), and the non-associated plastic potential function G^P is

$$197 \quad G^P = \left(\cos \theta + \frac{1}{\sqrt{3}} \sin \theta \sin \phi' \right) J \quad (18)$$

198 was assumed to limit dilatancy. The material parameters used for the two slopes are summarized in Table
 199 1.

200 **Convergence criteria for the coupled hydro-mechanical visco-plastic model**

201 Limit equilibrium and slip-line analyses are common methods for evaluating slope stability. The collapse
 202 zone or failure surface determined by slip-line method distinguishes this method from the limit
 203 equilibrium method, which considers the shear strength mobilized only a single failure surface. The failure
 204 zone can also be determined using a finite element approach with the SSRT. The loss of numerical

205 convergence or the onset of a sudden displacement are two typical methods to identify failure using a
206 finite element approach (Griffiths and Lane, 1999; Zienkiewicz et al. 2005; Hicks and Spencer, 2010)). In
207 solutions with coupled hydro-mechanical material models, non-convergence within a given number of FE
208 iterations can fail to detect the actual failure zone (Le et al. 2015). However, the sudden change of nodal
209 displacement during the gradual reduction of shear strength can be an effective method to predict the
210 failure as long as some rational criteria are selected.

211 In the investigation of Slope 1, Le et al. (2015) defined convergence criteria for identifying failure and
212 controlling the solution of the coupled hydro-mechanical visco-plastic model. Based on numerous finite
213 element analyses, they established three displacement criteria that could be determined numerically at
214 one or more surface nodes to identify a convergent failure condition. The FOS of the slope is then taken
215 as the largest strength reduction factor at which all 3 criteria are satisfied. For clarity in the subsequent
216 discussion, the three criteria identified by Le et al. (2015) are designated as follows:

- 217 1. **Relative Displacement Criterion** - The increment of either horizontal or vertical displacement
218 during one strength reduction step (i) of 0.01 exceeds 10 times the previous step ($i - 1$); ($\Delta x_i >$
219 $10 \times \Delta x_{i-1}$ or $\Delta y_i > 10 \times \Delta y_{i-1}$).
- 220 2. **Absolute Displacement Criterion** - Increment of total displacement > 2 mm during a strength
221 reduction step of 0.01.
- 222 3. **Cumulative Displacement Criterion** - The cumulative vertical or horizontal displacement > 10 mm.
223

224 Le et al. (2015) suggest that the first (Relative Displacement) criterion identifies failure as a sudden
225 increase in displacement, but criterion 2 (Absolute Displacement Criterion) assures that this does not
226 occur at very small absolute displacements. The third (Cumulative Displacement) criterion assures that a
227 considerable level of deformation has occurred and prevents any possible misleading reduction factor
228 during the early stages of the solution.

229 In this study, strength reduction steps of 0.01 were applied over a 2.5-day time interval, with the nodes
230 on the surface experiencing a gradual increase in displacement. The Absolute Displacement Criterion
231 was found to be satisfied at different displacements for the two different slope geometries and material

232 properties. For example, for Slope 1 the Absolute Displacement Criterion of 2 mm was met at the same
233 strength reduction step (problem time of about 52.5 days) as the Relative Displacement Criterion
234 (indicated by a greater than 10 times increase in displacement with the next strength reduction step of
235 0.01). This is illustrated in Fig. 3a where the total displacement of Point A on the crest of Slope 1 as a
236 function of problem time is shown as the strength reduction factor is increased. However in Slope 2,
237 different geometry and material properties result in a different critical point on the surface (Point B near
238 the toe), and the Relative Displacement Criterion was not met until the absolute displacement was 7
239 mm (Fig. 3b) at a problem time of 210 days, well past the time when the Absolute Displacement
240 criterion was met. In both slopes, when the Relative Displacement Criterion was satisfied, the
241 Cumulative Displacement Criterion was met, and the FOS was taken from the SSRT. The problem time
242 was then continued to further enhance the displacements and better define the failure zone.

243 In addition to these criteria, an additional criterion, referred to as the Rate of Displacement Change
244 Criterion, was implemented for this paper. The solution was assumed to have converged when the
245 change in displacement of a point on the slope surface from one step of the SSRT to the next was less
246 than 10^{-5} m/day, and was invoked regardless of the other three criteria. In Fig. 3 and subsequent figures
247 of FEM results, the conditions are depicted for the last strength reduction step for which the
248 convergence criteria are met, and the FOS is taken as the strength reduction factor.

249 **Factors affecting computational time**

250 The value of the viscosity of the soil has a significant effect on both the computation time and the
251 convergence of the visco-plastic model. To consider the effect of the assumed value of viscosity on the
252 computation time, Slope 1 was analyzed with viscosity values of 1 MPa.s, 100 MPa.s, and 100,000 MPa.s.,
253 with each value producing a different time to obtain convergence or "problem time" as well as different
254 computational times. Fig. 4 compares the results for the three different assumed viscosity values to

255 achieve a steady or convergent solution for the displacement of Point A on the top of Slope 1, and
256 indicates that the displacement solution is independent of the viscosity but the problem time as well as
257 the computational time varies significantly with the value of viscosity. The results of the convergence
258 study indicate that for a viscosity of 1 MPa.s., a convergent displacement was reached in a problem time
259 of about 0.01 day (Fig. 4), but 14 days of computational time was required. However, if the viscosity was
260 increased to an artificial viscosity of 10^2 MPa.s., the identical convergent displacement could be reached
261 in a problem time of 0.04 days but a computational time of only 4 days is required. Likewise, for an artificial
262 viscosity of 10^5 MPa.s., the computational time is reduced to only 0.04 days. Thus, by assuming an
263 artificially large value of viscosity, the computational time can be reduced significantly but the problem
264 time for displacement convergence also becomes artificial or fictitious. Since the time dependence of the
265 solution is not be important for these problems, the use of a fictitious time to facilitate the solution may
266 be convenient, and is consistent with that described by Zienkiewicz et al. (2005).

267 To place these viscosity values in context, reported experimental measurements on various soils yielded
268 a range of viscosity from 10^{-1} to 10^{10} MPa.s (Vyalov et al. (1986). A range of viscosity between 10^{-3} MPa.s.
269 and 5 MPa.s for different soils at various moisture contents was also reported (Ghezzehei and Or 2001;
270 Or and Ghezzehei 2002). Viscosity values of 5×10^{-2} to 3×10^{-1} MPa.s have been suggested for clay
271 loam soil (Karmakar and Kushwaha, 2007), while values of 10^{-4} to 5×10^{-1} MPa.s have been reported for
272 various soils below the liquid limit (Widjaja and Lee 2013).

273 The solution time increment is automatically controlled in CODE_BRIGHT. Because of the coupling
274 between the hydraulic and mechanical analysis, a time interval is specified during which the mechanical
275 forces, displacements, and hydraulic flux are calculated and allowed to come to equilibrium. The
276 computation time also increases as the time interval increases, and the effect of varying the time interval
277 required for the visco-plastic algorithm to converge was investigated. As shown in Fig. 5, the FOS reaches

278 a minimum value as the time interval is increased. Based on these analyses, a time interval of 2.5 days
279 was found to be sufficiently large for both Slope 1 and Slope 2 to satisfy all four of the above convergence
280 criteria.

281 **Results and Discussion:**

282 Results from the stability analyses conducted on the two planar slopes and their companion concave
283 slopes are shown in Figs. 6 through 11. For both Slope 1 (Fig. 6) and Slope 2 (Fig. 8) under gravity
284 loading, companion concave shapes were obtained using the equations proposed by Jeldes et al. (2013)
285 in Equations 2-5.

286 The reduced effective cohesion and effective friction angle (c^* and $\tan \phi^*$) required for the equations were
287 obtained from the original c' and $\tan \phi'$ divided by the FOS of the planar slopes under gravity load. Finite
288 element analysis confirmed that the concave slopes achieved essentially the same FOS under gravity alone
289 as the planar slopes. Both Slope 1 and Slope 2 concave shapes (Figs. 6b and 8b) exhibited a cusp or cliff at
290 the top of the slope where the largest displacements were concentrated, suggesting that the materials in
291 these zones may be most vulnerable to erosion or disturbance.

292 To investigate the effects of an unsaturated condition on the stability of the slopes, both the planar and
293 concave slopes were subjected to a 5 day period of drying or application of negative pore water pressure
294 through the boundary conditions on the slope as mentioned earlier. As expected, the FOS for both slopes
295 increased under the suction conditions, but the mode of potential slope failure became more deep-seated
296 as shown in Figs. 7 and 9. The distribution of the pore water pressure and suction obtained by mass water
297 balance equation in the slopes following drying period at $t=5$ days is shown in Fig. 10. The water flux (i.e.
298 water rate multiplied by a cross-sectional area) due to the hydraulic head (i.e. the gravitational head plus
299 the pore water pressure head) is shown in Fig. 11. The computation of direction and rate of water flux
300 indicates that Slope 2 (Figs. 11 (c) and (d)) is subjected to water flow from right to the left side of the slope

301 in a opposite direction (from negative pore water pressure toward positive pore water pressure) to
302 eliminate the overland flow generating positive pore pressure on the ground surface, whereas Slope 1
303 (Figs. 11 (a) and (b)) displays water flow in a level below the ground surface from positive pore pressure
304 zones to negative pore pressure zones directed from bottom to top of the water table.

305 Following the 5 day period of drying or application of the suction, a precipitation rate of 43.2 mm/day
306 (5^{-4} kg/m²/s) with duration of 5 days was applied through the ground surface. This rainfall event is
307 consistent with that investigated by Le et al. (2015). The loss of suction due to rainfall led to a decrease in
308 the factors of safety for both slopes and both planar and concave shapes. Figs. 12 and 13 suggest that the
309 failure zones after the precipitation event change little in Slope 2, but become more surficial in Slope 1,
310 and the concave Slope 1 appears to have a concentrated zone of large displacements in the portion near
311 the cusp.

312 The computed FOS from Figs. 6 – 9 and Figs. 12 and 13 are summarized in Table 2, and where applicable
313 compared with the FOS values reported from the literature for these slopes. The results shown in Table 3
314 indicate that while the Slope 1 and Slope 2 responded differently to the suction and rainfall events, each
315 of the concave slopes responded in a manner similar to their planar companion. This suggests that the
316 concave slopes will behave in a similar manner to the weather events as their equivalent planar slope, but
317 should maintain the advantages of the concave geometry with respect to erosion as identified by others.

318 **Evolution of Planar Slopes:**

319 To estimate how the shape of planar slopes may evolve over time due to erosion, it is assumed that the
320 large displacement failure zones within the slopes correspond to the portions where the soil particles may
321 be loose and detached and first susceptible to erosion during a rainfall event. It is recognized that this is
322 a very approximate means to represent soil loss due to erosion, and the resulting sediment is not re-
323 deposited at the toe. However, the focus was on the change in shape of the slope profile, especially in the

324 upper portion of the slope in the region of the mathematical or tension "cusp." Fig. 14 illustrates the
325 displacement time history of selected points on the surface and slightly below the surface of Slope 1. This
326 figure depicts the large displacements with time on the surface of the slope after applying the final
327 strength reduction increment of 0.01, reaching a maximum total nodal displacement of about 500 mm for
328 a problem time of 1400 days. The time history of several intermediate points below the surface is also
329 shown, with smaller displacements trending to a point on the interior where a more stable time history
330 at a displacement of about 10 mm is shown. It is assumed that the shape of the eroded slope can be
331 approximated by removing from the FE mesh the soil in this zone of unstable displacement history.

332 The two planar slopes 1 and 2 with the predicted zones of high displacement due to the first rainfall event
333 from Fig. 12a and 13a are repeated as Fig. 15a and 15b respectively, while Figs. 15c and 15d show the
334 resulting shape with the elements from the "eroded" zone removed by the method described above and
335 in Fig. 14. The new modified FE meshes were again loaded with the same initial gravity, suction, and
336 rainfall loadings described previously, and Figs. 15c and 15d show the computed displacements and zones
337 subject to erosion from the second weather event. Figs. 15e and 15f depict the slopes with the soil eroded
338 from the second weather event, and the response to a third cycle of gravity, suction and rainfall. The
339 rainfall/erosion effects on both slopes tend to transform the planar slope into a concave slope. The more
340 moderate Slope 1 in Fig. 15e suggests it is reaching a steady state concave shape after the third event,
341 while the steeper Slope 2 in Fig. 15f appears to be following the "parallel retreat" mode of failure (Jeldes
342 et al. 2018). These results also suggest that each suction/rainfall/erosion event is producing a slight
343 decrease in the computed level of safety or FOS.

344 **Evolution of Concave Shapes:**

345 The approach described above was taken to investigate how the shape of concave slopes would evolve
346 under the same sequence of drying/rainfall/erosion events. The concave shape corresponding to Slope 1

347 and Slope 2 was subjected to the 5 day period of drying followed by the 5 day precipitation event, and the
348 results from Fig. 12b and 13b are repeated as shown in Fig. 16a and 16b. The predicted zones of high
349 displacement or erosion susceptibility due to the rainfall event were removed as described above to
350 produce the slope shapes as shown in Figs. 16c and 16d, along with the high displacement zones due to
351 the second weather event. The shape was further modified as shown in Figs. 16e and 16f, and the
352 response to the third weather event is shown. It is noted that the second round of weather and slope
353 modification led to an increase in the stability or FOS for concave Slope 1 with the failure zone
354 concentrated around the cusp at the top of the slope, and the third round of loading and modification
355 resulted in no change in the FOS. However, while the stability increased from the first weather event to
356 the second in concave Slope 2, it decreased slightly due to the third event. As with the planar Slope 2, the
357 concave Slope 2 exhibited the parallel retreat response. Both concave slopes 1 and 2 were observed to
358 lose much of the cusp at the top of the slope due to the simulated rainfall/erosion events.

359 The responses in terms of the FOS's of Slope 1 (concave and planar) and Slope 2 (concave and planar) to
360 the three suction/rainfall/erosion weather events are summarized in Table 3. Although it is recognized
361 that the numerical differences between the various FOS values may not have much significance, some
362 relative differences and trends are observed. These changes in the computed FOS after the various
363 simulated drying/rainfall/erosion events are also shown in Fig. 17. It is noted that while the second and
364 third simulated erosion/rainfall events reduced the stability of the two planar slopes, these events had a
365 lesser effect on the stability of the concave slopes. This is in spite of the fact that the planar slopes
366 became more "concave-like" due to the simulated erosion, and suggests that for at least these two
367 slopes under the simulated weather and erosion events, the slopes designed to be concave may perform
368 better than the planar slopes.

369

370 **Conclusions:**

371 The mechanical stability of two planar slopes with different geometries and mechanical material
372 properties were investigated using a FE simulation with a coupled hydro-mechanical visco-plastic soil
373 model, and the Shear Strength Reduction Technique used to identify the factor of safety (FOS). Both planar
374 slopes were taken from the literature, with Slope 1 being of moderate inclination and being only
375 moderately stable in the absence of soil suction, and Slope 2 of more steep inclination. Companion
376 concave slopes were created from both planar slopes using the expression suggested by Jeldes et al.
377 (2013) to achieve slopes with approximately the same FOS under gravity. The convergence of the visco-
378 plastic soil model was investigated, as well as the effects of time interval and the assumed value of
379 viscosity on the solution.

380 The slopes were evaluated under gravity, and an arbitrary rainfall event preceded by an initial drying or
381 evaporation condition producing soil suction that was partially dissipated by the rainfall event. The results
382 indicate that while the two slopes responded differently to the suction and rainfall events, the two
383 concave slopes responded in a manner similar to their planar companion. This suggests that the concave
384 slopes will behave in a similar manner to the weather events as their equivalent planar slope, but should
385 maintain the advantages of the concave geometry with respect to erosion.

386 To investigate the evolution of slope cross-sectional shape due to the suction/rainfall/erosion cycles, it
387 was assumed that the portions of the slope with significant displacements would tend to be the areas
388 where the soil would have a tendency to erode. Although not intended to be a rigorous representation of
389 erosion and soil loss, this approximation should identify the soil zones with the highest degree of
390 erodibility. These erodible soil zones were removed from the mesh, creating a slope with modified cross
391 section. A sequence of three suction/rainfall/erosion cycles was found to transform both planar slopes
392 into concave slopes. The more moderate Slope 1 appeared to be tending towards a steady state concave

393 shape after the third event, while the steeper Slope 2 appeared to be following a "parallel retreat" mode
394 of failure.

395 A similar approach was taken to observe the evolution of the concave slopes due to the same sequence
396 of three suction/rainfall/erosion cycles. The results suggested that while the stability increased from the
397 first to the second weather event for both slopes, in concave Slope 1 the failure zone was concentrated
398 around the cusp at the top of the slope, and the third round of weathering/erosion resulted in no change
399 in the FOS. However, in concave Slope 2, the stability decreased due to the third event, and as observed
400 for the planar Slope 2, the concave Slope 2 exhibited a parallel retreat response. Both concave slopes 1
401 and 2 were observed to lose the cusp at the top of the slope due to the simulated rainfall/erosion events.
402 It was noted that while the second and third simulated erosion/rainfall events reduced the stability of the
403 two planar slopes, these weather events had a lesser effect on the stability of the concave slopes. This is
404 in spite of the fact that the planar slopes became more "concave-like" due to the simulated erosion, and
405 suggests that for at least these two slopes under the simulated weather and erosion events, the slopes
406 designed to be concave may perform better than the planar slopes.

407 **Data Availability Statement:**

408 Some or all data, models, or code generated or used during the study are available in a repository or online
409 in accordance with funder data retention policies. Input files used with the Code_Bright (DIT-UPC, 2015)
410 analyses will be available at Tennessee Research and Creative Exchange (TRACE)
411 <https://www.trace.tennessee.edu/> which is the University of Tennessee's institutional open-access
412 repository.

413

414 **References:**

- 415 Cai, F. and Ugai, K. (2004) "Numerical Analysis of Rainfall Effects on Slope Stability." *International Journal*
416 *of Geomechanics*, 4(2). doi:10.1061/(ASCE)1532-3641(2004)4:2(69).
- 417 DIT-UPC (2015). "CODE_BRIGHT." A 3-D Program for Thermo-hydro-mechanical Analysis in Geological
418 Media, The Department of Geotechnical Engineering and Geosciences of the Universitat
419 Polit cnica de Catalunya.
- 420 Ghezzehei, T.A., and Or, D. (2001). "Rheological properties of wet soils and clays under steady and
421 oscillatory stresses." *Soil Sci. Soc. Am. J.* 65, 624-637. Gray, D. (2013). "Influence of slope
422 morphology on the stability of earthen slopes." In *Proceedings of Geo-Congress 2013*. pp. 1895-
423 1904. doi:10.1061/9780784412787. 191.
- 424 Griffiths, D.V., and Lane, P.A. (1999). "Slope stability analysis by finite elements." *G otechnique*, 49(3):
425 387–403. doi:10.1680/geot.1999.49.3.387
- 426 Hancock, G.R., Loch, R.J., and Willgoose, G.R. (2003). "The design of post-mining landscapes using
427 geomorphic principles." *Earth Surface Processes and Landforms* 28: 1097-1110.
428 DOI:10.1002/esp.518.
- 429 Hicks, M.A., and Spencer, W.A. (2010). "Influence of heterogeneity on the reliability and failure of a long
430 3D slope." *Computer and Geotechnics*, 37(7-8): 948–955. doi:10.1016/j.compgeo.2010.08.001
- 431 Jeldes, I.A., Vence, N.E., and Drumm, E.C. (2013). "Approximate solution to the Sokolovskii concave slope
432 at limiting equilibrium." *International Journal of Geomechanics*, 15(2).
433 doi:10.1061/(ASCE)GM.1943-5622.0000330.
- 434 Jeldes, I.A, Drumm, E., and Yoder, D. (2015). "Design of stable concave slopes for reduced sediment
435 delivery." *Journal of Geotechnical and Geoenvironmental Engineering*, 141(2).
436 doi:10.1061/(ASCE)GT.1943-5606.0001211.
- 437 Jeldes, I. A., Yoder, D.C., and Drumm, E.C. (2018) "Sustainable Slopes: Satisfying Rainfall-Erosion
438 Equilibrium and Mechanical Stability" *Transactions of the ASABE, American Society of Agricultural*
439 *and Biological Engineers* Vol. 61(4): 1323-1333
- 440 Karmakar S, and Kushwaha R.L. (2007). "Development and laboratory evaluation of a Rheometer for soil
441 visco-plastic parameters. *J. Terramech*; 44:197–204.
- 442 Le, T.M.H., Gallipoli, D., Sanchez, M., and Wheeler, S.J. (2015). "Stability and failure mass of unsaturated
443 heterogeneous slopes." *Canadian Geotechnical Journal*, 52(11): p. 1747-1761.
- 444 Le, T. M. H., Gallipoli, D., Sanchez, M., and Wheeler, S. (2016). "Characteristics of failure mass and safety
445 factor during rainfall of an unsaturated slope." *E3S Web of Conferences UNSAT 9*, 15011 (2016).
446 DOI: [https://doi.org/ 10.1051/e3sconf/20160915011](https://doi.org/10.1051/e3sconf/20160915011).
- 447 Nelson, J.D., Overton, D.D. and Durkee, D.B. (2001). "Depth of Wetting and the Active Zone." *Expansive*
448 *Clay Soils and Vegetative Influence on Shallow Foundations*, ASCE, Houston, Texas, USA: pp. 95-
449 109.
- 450 Or, D., and Ghezzehei, T.A. (2002). "Modeling post-tillage soil structural dynamics: a review." *Soil Tillage*
451 *Res.* 64, 41-59.
- 452 Schor, H. J., and Gray, D. H. (2007). *Landforming: an environmental approach to hillside development,*
453 *mine reclamation and watershed restoration*. John Wiley & Sons, Hoboken, NJ.
- 454 Sokolovskii, V. V. (1960). *Statics of soil media*, Butterworths, London.
- 455 Sokolovskii, V. V. (1965). *Statics of granular media*, Pergamon Press, New York.
- 456 Utili, S. and Nova, R. (2007). "On the optimal profile of a slope." *Soils and Foundations*. 47, No. 4, 717–
457 729.

458 Vahedifard, F., Shahrokhbabadi, S., and Leshchinsky, D. (2016). "Optimal profile for concave slopes under
459 static and seismic conditions." *Canadian Geotechnical Journal*, 53(9), 1522-1532. doi:10.1139/cgj-
460 2016-0057.

461 van Genuchten, M.T. (1980). "A closed-form equation for predicting the hydraulic conductivity of
462 unsaturated soils." *Soil Science Society of America Journal*, 44, 892-898.
463 doi:10.2136/sssaj.03615995004400050002x.

464 Vo, T. and Russell, A. R. (2017) "Stability charts for curvilinear slopes in unsaturated soils." *Soils and*
465 *Foundations*, Volume 57, Issue 4, August 2017, Pages 543-556

466 Vyalov SS. (1986). *Rheological fundamentals of soil mechanics*. Elsevier Science Publishing Company,
467 Amsterdam, The Netherlands.

468 Widjaja, B., and Lee, S.H. (2013) "Flow box test for viscosity of soil in plastic and viscous liquid states"
469 *Soils and Foundations*, Volume 53, Issue 1, February 2013, Pages 35-46.

470 Zienkiewicz OC, Humpheson C, and Lewis RW. (1975). "Associated and non-associated visco-plasticity in
471 soil mechanics." *Géotechnique*, 25(4):671-689.

472 Zienkiewicz, O.C., Taylor, R.L., and Zhu, J.L. (2005). *The finite element method: its basis and*
473 *fundamentals*. 5th ed. McGraw-Hill, Oxford.

474
475
476
477
478
479
480
481
482
483
484
485
486
487
488
489
490
491
492
493
494
495
496
497
498
499
500
501
502
503
504
505

506
507
508

509 **Fig. 1.** Slope geometry, water table, applied boundary conditions, and meshing:

510 a) Slope 1 (after Le et al. 2015, 2016) and b) Slope 2 (after Jeldes et al. 2015)

511 **Fig. 2.** Soil water characteristic curve (a) and unsaturated hydraulic conductivity permeability

512 function (b) assumed for the slopes.

513 **Fig. 3.** Maximum total displacement evolution using shear strength reduction factor technique at (a)

514 point A for Slope 1 and (b) point B for Slope 2. The vertical red line indicates the last strength reduction

515 step before the Relative Displacement Criterion convergence criterion is satisfied.

516 **Fig. 4.** Problem time for the total displacement of Point A (Fig. 3) for different viscosities of the soil

517 matrix in Slope 1

518 **Fig. 5.** Effect of time interval on the factor of safety for Slope 1 (a, b) and for Slope 2 (c, d) under gravity

519 loading only and both gravity and suction loading, respectively

520 **Fig. 6.** Total displacement contour and factor of safety under gravity load of Slope 1 (a) planar (b)

521 concave

522 **Fig. 7.** Total displacement contour and factor of safety under gravity and suction loads of Slope 1 (a)

523 planar (b) concave

524 **Fig. 8.** Total displacement contour and factor of safety under gravity load of Slope 2 (a) planar (b)

525 concave

526 **Fig. 9.** Total displacement contours and factor of safety under gravity and suction loads of Slope 2 (a)

527 planar (b) concave

528 **Fig. 10.** Distribution of pore water pressure/suction in slopes following drying period at time = 5 days: a)

529 Slope 1 planar, b) Slope 1 concave, c) Slope 2 planar, d) Slope 2 concave

530 **Fig. 11.** Computed hydraulic flux in slopes following drying period at time = 5 days: a) Slope 1 planar, b)
531 Slope 1 concave, c) Slope 2 planar, d) Slope 2 concave

532 **Fig. 12.** Total displacement contours and factor of safety under gravity and suction loads followed by the
533 precipitation event: Slope 1 (a) planar (b) concave

534 **Fig. 13.** Total displacement contours and factor of safety under gravity and suction loads followed by the
535 precipitation event Slope 2 (a) planar (b) concave

536 **Fig. 14.** Total displacement versus time at various points in the failure zone of Slope 1, used for the
537 identification of eroded soil zones

538 **Fig. 15.** Evolution of planar slopes from first to third rainfall events: Planar Slope 1 (figures a, c, and e)
539 and Planar Slope 2 (figures b, d, and f)

540 **Fig. 16.** Evolution of concave slopes from first to third rainfall events: Concave Slope 1 (figures a, c, and
541 e) and Concave Slope 2 (figures b, d, and f)

542 **Fig. 17.** Effect of drying/rainfall/erosion event on the computed factor of safety of planar and concave
543 slopes 1 and 2

544

545

546

547

548

549

550

551

552

553

554

Table 1. Mechanical and hydraulic soil properties used in Slopes 1 and 2

Mechanical Parameters				Hydraulic Parameters		
Symbol	Parameter name	Value		Symbol	Parameter name	Value (Slope 1 & Slope 2)
		Slope 1	Slope 2			
E	Elastic Modulus (MPa)	100	20	m	Shape function for retention curve	0.2
ν	Poisson's ratio	0.3	0.3	η	Parameter for porosity influence on retention curve	5
K_s	Bulk Modulus against suction changes (MPa)	10^7	10^7	S_s	Maximum saturation	1
ρ_t	Total density (kg/m^3)	1800	1900	S_r	Residual saturation	0.001
c'	Effective cohesion (kPa)	5	15	K	Intrinsic permeability (m^2)	10^{-12}
ϕ', ϕ^b	Effective friction angles (degree)	20, 18	35, 18	k_{so}	Saturated permeability (m/s)	10^{-5}
n_0	Initial Porosity	0.33	0.296	S_{e0}	Reference air-entry pressure (kPa)	20
η^M	Viscosity* (MPa.s.)	10^5	10^5	γ_l	Leakage Coefficient	-10
p_t	Soil Tensile Strength (kPa)	13.7	21.4	μ_l	Water viscosity, (MPa.s.)	10^{-9}
p_{lo}	Reference water pressure (kPa)	100	100	ρ_l	Density of water (kg/m^3)	10^3

555 *Note: The viscosity value was not reported by Le et al. (2015 and 2016)

556

557

558

559

560

561

562

Table 2. Computed Factor of Safety for Slopes 1 and 2

Slope	FOS - Gravity only, before suction		FOS - with suction		FOS - with rainfall	
	This study	Literature solution	This study	Literature solution	This study	Literature solution
1 (Planar)	1.16	---	1.98	1.95 (Le et al. 2015)	1.66	1.70 (Le et al. 2015)
1 (Concave)	1.17	---	2.05	---	1.71	---
2 (Planar)	1.43	1.50 (Jeldes et al. 2015)	1.79	---	1.69	---
2 (Concave)	1.44	1.51 (Jeldes et al. 2015)	1.74	---	1.64	---

563

564

Table 3. Changes in Factor of Safety for Slopes 1 and 2 due to Weather Events 1, 2 and 3

Slope	FOS Gravity only	FOS due first drying/rainfall event	FOS due second drying/rainfall event	FOS due third drying/rainfall event
Weather Event	-	1	2	3
Slope 1 (Planar)	1.16	1.66	1.58	1.36
Slope 1 (Concave)	1.17	1.71	1.78	1.78
Slope 2 (Planar)	1.43	1.69	1.62	1.58
Slope 2 (Concave)	1.44	1.64	1.90	1.62

565

566

567

568

569

